Calibration of spectral line data at the IRAM 30m radio telescope

C. Kramer

January 24th, 1997, Version 2.1

IRAM
Instituto de Radioastronomia Milimétrica
Avenida Divina Pastora 7, Núcleo Central
18012 Granada, España

This report describes in detail the steps involved when deducing the brightness temperature of an astronomical source from the backend counts detected. It supplements already existing texts of Downes (1989) and Guilloteau (1987, 1993).
The calibration procedure has to take into account backend and receiver gains and, possibly, drifts, atmospheric transmission and variations, pointing and focus deviations, losses due to diffraction, spillover, scattering, blockage, etc.. It is obvious that this can never be done perfectly. The atmospheric attenuation, in particular, is the main source of spectral calibration uncertainty.
The first chapter deals with the derivation of the receiver temperature from two loads of known temperatures. The second chapter describes the 'chopper wheel' calibration procedure implemented in the observing program at the 30m telescope, `OBS` . The formulas needed are derived. The derivation of efficiencies and beam widths is the topic of the third chapter. These quantities are needed to determine the telescope performance and to derive beam averaged brightness temperatures. Chapter 4 gives recommendations on which planets to use as standard calibrators and presents their brightness temperatures known from the literature. These temperatures and formula were implemented in a program to calculate fluxes and efficiencies. It is currently used for the reduction of planetary scans obtained during the regular pointing sessions at the 30m telescope. Chapter 5 presents measured 30m telescope parameters, i.e. half power beam widths and efficiencies. The derived values are consistent with a subreflector edge taper of 11 ± 3 dB, for all five receivers in the frequency range 90 to 240 GHz and beyond. In addition, the measured aperture efficiencies are consistent with a main dish tapered surface accuracy of σ_s=85 μm. A discussion of the errorbeam is referred to Greve, Kramer, Wild (1997).

Contents

1 The receiver temperature

1.1 The definition

In order to relate backend counts to antenna temperatures, at least two sources of known temperature and output counts are needed. In a first step of the calibration procedure the counts on a hot load (the chopper) at approximately room temperature and the counts on a cold load at approximately the temperature of liquid nitrogen are measured and averaged over the channels of the specific backend used. For a perfectly linear detector, the output counts C of the chopper and cold load signals are proportional to the input temperatures T:

$$\begin{aligned} \langle C_{\rm chop}\rangle &= \langle c_{\rm off}\rangle + (T_{\rm chop} + T_{\rm rec}) * g \\ \langle C_{\rm cold}\rangle &= \langle c_{\rm off}\rangle + (T_{\rm cold} + T_{\rm rec}) * g, \end{aligned}$$

where g is the variing gain factor to be calibrated out. "Dark counts", that is a constant offset $\langle c_{\rm off}\rangle$, possibly arise in some of the backends even when no frontend signal is fed in. The receiver noise temperature is thus given by

$$\begin{aligned} T_{\rm rec} &= \frac{T_{\rm cold}\langle C_{\rm chop}\rangle - T_{\rm chop}\langle C_{\rm cold}\rangle}{\langle C_{\rm cold}\rangle - \langle C_{\rm chop}\rangle} - \langle c_{\rm off}\rangle \frac{T_{\rm chop} - T_{\rm cold}}{\langle C_{\rm chop}\rangle - \langle C_{\rm cold}\rangle} \\ &= \frac{T_{\rm chop} - Y T_{\rm cold}}{Y - 1} \qquad \text{with} \qquad Y = \frac{\langle C_{\rm chop}\rangle - \langle c_{\rm off}\rangle}{\langle C_{\rm cold}\rangle - \langle c_{\rm off}\rangle}. \end{aligned} \tag{1}$$

This temperature is needed to evaluate the performance of the receiver, including parts of the optics and the backend but without having to consider atmospheric influences. Depending on the placing of the loads within the signal path, the receiver temperature will vary and will include some optical losses. Receiver temperatures are overestimated when backend dark counts $\langle c_{\rm off}\rangle$ are considerable and not taken into account.

1.2 The procedure applied

The counts on the internal cold and hot load are measured automatically during a calibration. Their physical temperatures are known but have to be corrected for the fact that the receiver also receives some radiation of the ambient environment when 'looking' at a load. This 'spillover' is dependent on the receiver and on the tuned frequency.
To get the correct cold load temperature an external cold and afterwards an external hot load are positioned by hand at the reference plane which is in front of the first beam splitter of the receiver optics. This should be done once in a while to check the cold load temperature of the automatic calibration system. The output counts $C^{\rm ext}_{\rm cold}$ and $C^{\rm ext}_{\rm chop}$ of the continuum backend are recorded. The external cold load is a piece of `ECCOSORB` which was immersed into liquid nitrogen. The radiation temperature of this external load is estimated to be $T^{\rm ext}_{\rm cold} = T_N$, the temperature of liquid nitrogen. The external hot load is another piece of `ECCOSORB` at room temperature. The room temperature $T_{\rm room}$ in the receiver cabin is measured regularly by a temperature sensor PT100 and is input automatically into `OBS` , the observing program at the 30m telescope.
With the externally measured counts $C^{\rm ext}_{\rm cold}$, $C^{\rm ext}_{\rm chop}$, and the known physical temperatures of the loads, a 'correct' receiver temperature $T^{\rm corr}_{\rm rec}$ is derived:

$$T^{\rm corr}_{\rm rec} = \frac{T_{\rm chop} - Y^{\rm ext} T^{\rm ext}_{\rm cold}}{Y^{\rm ext} - 1} \qquad \text{with} \qquad Y^{\rm ext} = \frac{C^{\rm ext}_{\rm chop} - \langle c_{\rm off}\rangle}{C^{\rm ext}_{\rm cold} - \langle c_{\rm off}\rangle}$$

Next, the Y-factor, $Y = (\langle C_{\rm chop}\rangle - \langle c_{\rm off}\rangle)/(\langle C_{\rm cold}\rangle - \langle c_{\rm off}\rangle)$, for the internal loads of the automatic calibration system is measured and the corrected internal cold load temperature is calculated:

$$T_{\rm cold}^{\rm corr} = \frac{T_{\rm chop} - (Y-1)T_{\rm rec}^{\rm corr}}{Y}$$

The internal chopper load also is an ECCOSORB absorber, its temperature is taken to be equal to room temperature: $T_{\rm chop} = T_{\rm room}$.
The corrected cold load temperature $T_{\rm cold}^{\rm corr}$ has to be given by the observer into OBS . The calibration routines can thus calculate the 'correct' receiver temperatures and 'correct' antenna temperatures when doing a standard CAL COLD measurement:

$$T_{\rm rec} = \frac{T_{\rm chop} - YT_{\rm cold}^{\rm corr}}{Y-1}$$

This receiver temperature refers to the backend/receiver/optics chain up to the reference plane.

The temperature of liquid nitrogen at sea level is $T_{N,0} = 77.36$ K. This temperature is related to the barometric pressure P in [mmHg] by $T_N = T_{N,0} + 0.011(P - 760)$ [K] (Ulich et al. 1980). The temperature of liquid nitrogen at the altitude of the IRAM 30m RT is thus reduced to $T_N = 75$ K.

1.3 Comments

The above procedure relies on several assumptions:
• All loads are 'black bodies' and the physical temperature of the loads are equivalent to their Rayleigh-Jeans radiation temperatures, that is $h\nu \ll kT$. For a load with a brightness temperature T_B of 77 K the correct Planck radiation temperature $J_\nu(T_{\rm B}) = h\nu/k(\exp(h\nu/kT_{\rm B}) - 1)^{-1}$ at 345 GHz is 70 K. This 10% difference would, if taken into account, result in a 10% higher receiver temperature. Assuming a $T_{\rm rec}$ of 100 K, Guilloteau (1993) showed that a 10 K error in $T_{\rm rec}$ would induce a variation of only 0.3% in the antenna temperatures. It is thus acceptable to use the Rayleigh-Jeans approximation. • The temperature conductancy of the external cold load is high enough, that the cold load really has a physical temperature of T_N at its entire radiating surface. • The ambient temperature measured within the receiver cabin is the same as that of the hot load piece of ECCOSORB. This might be not the case when, e.g., the hot load scatters radiation from the sky or from the cold load into the beam, but there is no indication for this error at the 30m RT. • Counts are directly proportional to the incoming power. The linearity of the receivers is checked. Up to now (February 3, 1997) backend offsets are not taken into account. • The amplification of the system does not change on timescales smaller than the calibration procedure.

2 The calibration method

2.1 The sky

To translate counts $\langle C_{\rm atm}\rangle$ measured on the sky into the antenna temperature on the sky $T_{\rm A}^{\rm sky}$ ($\equiv T_{\rm emi}$ in OBS) we use:

$$\frac{T_{\rm chop} - T_{\rm A}^{\rm sky}}{\langle C_{\rm chop}\rangle - \langle C_{\rm atm}\rangle} = \frac{T_{\rm chop} - T_{\rm cold}^{\rm corr}}{\langle C_{\rm chop}\rangle - \langle C_{\rm cold}\rangle}. \qquad (2)$$

Backend counts $\langle c_{\rm off}\rangle$ cancel out when solving for $T_{\rm A}^{\rm sky}$ as well as the first order Rayleigh-Jeans correction.

The antenna temperature $T_{\rm A}^{\rm sky}$ measured pointing toward the sky is a composition of the effective brightness temperature of the sky $T_{\rm sky}$ and the temperature of the 'cabin', $T_{\rm cab}$:

$$T_{\rm A}^{\rm sky} = F_{\rm eff} T_{\rm sky} + (1 - F_{\rm eff}) T_{\rm cab} \qquad \Leftrightarrow \qquad T_{\rm sky} = ... \qquad (3)$$

At the 30m telescope, the cabin temperature $T_{\rm cab}$ ($\equiv T_{\rm spill}$ as defined by Kutner & Ulich (K&U), 1981) is estimated to be a weighted average of the outside temperature and the chopper load temperature : $T_{\rm cab} = 0.8\ T_{\rm chop} + 0.2\ T_{\rm amb}$.

The forward efficiency $F_{\rm eff}$ (see K&U, Downes 1989) is derived from a skydip by a subsequent fit of a model function to the measured antenna temperatures of the sky at different elevations (see §3.5). See Downes (1989) for a comparison of $F_{\rm eff}$ with the efficiencies defined in K&U, $\eta_{\rm l} = \eta_{\rm r}\eta_{\rm rss}$.

An atmospheric model (`ATM`: Cernicharo 1988) is used to fit the emission of both receiver sidebands to the sky temperature $T_{\rm sky}$ (eq. 3) by variing the amount of water vapour and taking into account the sideband gain ratio. The water vapour content of the atmosphere thus derived, together with the local pressure and temperature measured by the weather station, are used to calculate the sky temperature within the two sidebands ($T_{\rm sky}^{\rm s}$, $T_{\rm sky}^{\rm i}$) and the corresponding atmospheric opacities ($\tau_{\rm s}$, $\tau_{\rm i}$).

By modelling correctly the atmospheric emission, the atmospheric transmission can thus be derived. The model uses a standard atmosphere and the equation of radiative transfer to compute the total absorption and thermal emission by water vapour and oxygen through the atmosphere.

The sky temperature $T_{\rm sky}$ is the sum of the contribution of the two sidebands weighted by the sideband gain ratio $G_{\rm im} = G_{\rm i}/G_{\rm s}$ (averaged over the receiver bandwidth), and normalized such that $G_{\rm i} + G_{\rm s} = 1$:

$$T_{\rm sky} = G_{\rm s} T_{\rm sky}^{\rm s} + G_{\rm i} T_{\rm sky}^{\rm i} \qquad \Leftrightarrow \qquad T_{\rm sky} = \frac{T_{\rm sky}^{\rm s} + T_{\rm sky}^{\rm i} * G_{\rm im}}{1 + G_{\rm im}} \qquad (4)$$

2.1.1 Comments

The version of `ATM` installed at the 30m telescope takes into account the atmospheric absorption by water and oxygen. At most frequencies in the millimeter regime these two molecules are the most important absorbing species in the atmosphere; for high-altitude sites and for low amounts of precipitable water vapour the contribution of Ozone may however be important. A standalone version of `ATM` which takes account the contribution of Ozone lines, is available at the telescope.

For a perfect model, the water vapour values measured in one calibration scan at different frequencies should all be equal since they are derived from a simultaneous measurement of the sky temperature $T_{\rm sky}(\nu)$ along the same line of sight. Deviations between water vapour values, derived from scans at different frequencies which were taken simultaneously, do **not** indicate calibration errors.

2.2 Spectral line calibration

2.2.1 Formulas used

The calibration method applied at the IRAM observatories, often called the 'chopper wheel method', uses the sky, the hot load, and indirectly also the cold load as calibration sources. Essentially the difference of counts between the source and the blank sky (the off position) $C_{\rm source} - C_{\rm atm}$ is related to the difference of counts between the hot load and the blank sky $C_{\rm chop} - C_{\rm atm}$:

$$T^*_{{\rm A},i} = T_{\rm cal} * \frac{C_{{\rm source},i} - C_{{\rm atm},i}}{C_{{\rm chop},i} - C_{{\rm atm},i}} = T_{\rm cal} * \frac{\Delta C_{{\rm source},i}}{\Delta C_{{\rm cal},i}} = T_{\rm cal} * \frac{{\rm signal}_i}{{\rm gain}_i}. \qquad (5)$$

This calculation is done for each backend channel i. All counts are weighted according to the corresponding integration times.
The calibration factor $T_{\rm cal}$ is given by:

$$T_{\rm cal} = \frac{(1 + G_{\rm im})}{F_{\rm eff} * \exp(-\tau_{\rm s} A)} * (T_{\rm chop} - T^{\rm sky}_{\rm A}) \qquad \text{for spectral line observations} \qquad (6)$$

with the antenna temperature on the sky $T^{\rm sky}_{\rm A}$ (calculated from eqs. (3, 4),
the hot (chopper) load temperature $T_{\rm chop}$,
the gain ratio of the two sidebands $G_{\rm im} = G_{\rm i}/G_{\rm s}$ (called `GAIN_IMAGE` in `OBS`),
the signal band zenith opacity $\tau_{\rm s}$,
and the airmass at elevation El $A = 1/\sin(El)$.

The $T^*_{\rm A}$ temperatures are brightness temperatures of an equivalent source which fills the entire 2π sterradians of the forward beam pattern of the telescope.
To obtain the brightness temperature of an equivalent source just filling the main beam (defined as main beam brightness temperature T_{mb}), antenna temperatures have to be multiplied by the ratio of the forward and the main beam efficiency $B_{\rm eff}$ (§3.4). See Downes (1989) for a comparison with the forward spillover and scattering efficiency ($\eta_{\rm fss}$) defined by K&U.

$$T_{\rm mb} = \frac{F_{\rm eff}}{B_{\rm eff}} T^*_{\rm A}$$

This is equivalent to using $B_{\rm eff}$ instead of $F_{\rm eff}$ in eq. (6) (see `OBS`).
The main beam efficiency is usually derived from continuum observations of planets, whose disk radiation temperature is known, and whose angular diameter fills the main beam.

2.2.2 Derivation of the formula for the calibration temperature $T_{\rm cal}$

The 'chopper-wheel' calibration method is described by Ulich & Haas (1976), Ulich (1980), and K&U. See also Downes (1989). The following part summarizes the deviation of the calibration factor $T_{\rm cal}$. The only assumption used is that the radiation temperatures in both sidebands are equal: $J(\nu_{\rm s}, T) = J(\nu_{\rm i}, T) = J(T)$ for all temperatures T.
The counts detected by the receiver when looking at the hot load (the chopper) are
$C_{\rm chop} = g\left[G_{\rm s} J(\nu_{\rm s}, T_{\rm chop}) + G_{\rm i} J(\nu_{\rm s}, T_{\rm chop}) + T_{\rm rec}\right]$ where g again is the variing receiver gain factor. We do not have to take into account losses due to spillover, since the load is at

room temperature. Backend offsets are neglected since they will always cancel out when calculating antenna temperatures (see eq. 5).
The counts detected when looking at the blank sky are:

$$\begin{aligned} C_{\rm atm} &= g\Big(G_{\rm s}\Big[F_{\rm eff}J(\nu_{\rm s},T_{\rm sky})+(1-F_{\rm eff})J(\nu_{\rm s},T_{\rm cab})\Big] \\ &\quad +G_{\rm i}\Big[F_{\rm eff}J(\nu_{\rm i},T_{\rm sky})+(1-F_{\rm eff})J(\nu_{\rm i},T_{\rm cab})\Big]+T_{\rm rec}\Big). \end{aligned}$$

For each sideband the radiation of the sky is the sum of the average sky temperature $T_{\rm ATM}$ and the cosmic background radiation temperature $T_{\rm bg}$:
$J(\nu,T_{\rm sky}) = J(\nu,T_{\rm ATM})(1-\exp(-\tau A)) + J(\nu,T_{\rm bg})\exp(-\tau A)$.
With this, the numerator in eq. (5), $\Delta C_{\rm cal} = C_{\rm chop} - C_{\rm atm}$, is derived.

Antenna temperatures $T_{\rm A}^*$, corrected for atmospheric attenuation, the forward efficiency, and the signal band gain are

$$T_{\rm A}^* = T_{\rm A}\exp(\tau_{\rm s}A) * \frac{1}{G_{\rm s}F_{\rm eff}} = T_{\rm A}'\frac{1}{F_{\rm eff}},$$

if the signal to be observed is only detected in the signal band. The antenna temperature $T_{\rm A}$ is derived from the counts and load temperatures via eq. (2). We thus have
$\Delta C_{\rm source} = C_{\rm source} - C_{\rm atm} = gT_{\rm A} = gG_{\rm s}F_{\rm eff}\exp(-\tau_{\rm s}A)T_{\rm A}^*$.
The calibration factor $T_{\rm cal}$ is now defined such that

$$T_{\rm cal} = \frac{\Delta C_{\rm cal}}{\Delta C_{\rm source}} * T_{\rm A}^* = \frac{\Delta C_{\rm cal}}{gG_{\rm s}F_{\rm eff}\exp(-\tau_{\rm s}A)} \tag{7}$$

and we finally find:

$$\begin{aligned} T_{\rm cal} &= (1+G_{\rm im})\Big[J(\nu_{\rm s},T_{\rm ATM})-J(\nu_{\rm s},T_{\rm bg})\Big] \\ &\quad +(1+G_{\rm im})\Big[J(\nu_{\rm s},T_{\rm cab})-J(\nu_{\rm s},T_{\rm ATM})\Big]\exp(\tau_{\rm s}A) \\ &\quad +G_{\rm im}\Big[J(\nu_{\rm s},T_{\rm ATM})-J(\nu_{\rm s},T_{\rm bg})\Big]\Big[\exp((\tau_{\rm s}-\tau_{\rm i})A)-1\Big] \\ &\quad +(1+G_{\rm im})/F_{\rm eff}\Big[J(\nu_{\rm s},T_{\rm chop})-J(\nu_{\rm s},T_{\rm cab})\Big]\exp(\tau_{\rm s}A) \end{aligned} \tag{8}$$

Note that g and $T_{\rm rec}$ cancel out. This formula is identical to eq. (A12) of K&U. It is a more general form of the calibration factor of the chopper wheel method than eq. (6).

2.2.3 Comments

Note that for historical reasons the hot load is called chopper and the calibration method applied here is called 'chopper wheel' calibration. These names can be misleading because the beam switch mirror, which switches between positions on the sky 70″ apart, is often called 'chopper wheel' but is totally unrelated to the hot load or the calibration method.

The above formula equals the formula used at IRAM (eq. 6), with $\eta = F_{\rm eff}$, on the assumption that the Rayleigh-Jeans approximation is valid and that the background temperature is negligible: $J(T) = T$ ($h\nu \ll kT$) for all temperatures and frequencies and $T_{\rm bg} = 0$. The radiation temperature can be estimated by $J_\nu(T_{\rm B}) = T_{\rm B} - \frac{h\nu}{2k}$ with an error of less than 3% for $h\nu/k \leq 0.5T_{\rm B}$ ($h\nu/k$ is 11.0 K at 230 GHz). Note that these first order Rayleigh-Jeans correction terms would all cancel out in eq. (8).

2.3 Continuum calibration

In the above derivation of the calibration factor $T_{\rm cal}$ of the 'chopper wheel method' it was assumed that the signal comes only from the signal sideband and not from the lower - **and** upper sideband.
If the signal comes from both sidebands as is the case for continuum emission sources then we have to use

$$T_{\rm cal} = \frac{\Delta C_{\rm cal}}{\Delta C_{\rm source}} * T_{\rm A}^{*} = \frac{\Delta C_{\rm cal}}{g G_{\rm s} F_{\rm eff} \exp(-\tau_{\rm s} A) + g G_{\rm i} F_{\rm eff} \exp(-\tau_{\rm i} A)}$$

instead of eq. (7).
Or equivalently antenna temperatures, $T_{\rm A}^{*}$, calculated with eq. (6) must be multiplied by a factor

$$\left(1 + G_{\rm im} \exp((\tau_{\rm s} - \tau_{\rm i}) A)\right)^{-1}.$$

This is done automatically within `OBS` during continuum observations.
The factor equals 0.5 if the sideband gain ratio is one (double sideband operation) and the opacities in the two sidebands both are equal.
The calibration factor $T_{\rm cal}$ no longer depends directly on the sideband ratio $G_{\rm im}$ for the case of equal opacities in both sidebands, i.e. $\tau_s = \tau_i$. The sideband ratio $G_{\rm im}$ is however used by the atmospheric model `ATM` to calculate the signal band opacity.

2.4 Spectral line observations in the image sideband

If the signal comes from the image sideband we have to use $T_{\rm cal} = \Delta C_{\rm cal} / g G_{\rm i} F_{\rm eff} \exp(-\tau_{\rm i} A)$ instead of eq. 7. If you are thus interested in the image band, you have to multiply the antenna temperatures from eq. (6) by a factor

$$G_{\rm im}^{-1} \exp((\tau_{\rm i} - \tau_{\rm s}) A).$$

2.5 The system temperature

To evaluate the noise performance of the receiver plus the atmosphere a formula for the system temperature $T_{\rm sys}$ can be derived from the above formulae (we assume here that the signal is detected only in the signal band of the receiver):

$$T_{\rm sys} = \frac{(1 + G_{\rm im})}{F_{\rm eff} \exp(-\tau_{\rm s} A)} \Big[F_{\rm eff} T_{\rm sky} + (1 - F_{\rm eff}) T_{\rm cab} + T_{\rm rec} \Big]$$

or equivalently (within `OBS`):

$$T_{\rm sys} = T_{\rm cal} * \frac{\langle C_{\rm atm} \rangle}{\langle C_{\rm chop} \rangle - \langle C_{\rm atm} \rangle}$$

Note that the values for the receiver and the system temperature are dependent on the part of the IF-Band used. The receiver and the system temperature both tend to be too high when backend dark counts $\langle c_{\rm off} \rangle$ are not accounted for.

3 Aperture -, main beam efficiency, and beam width

The accurate knowledge of efficiencies and the beampattern is essential in order to estimate source brightness temperatures and to interpret the data taken with the telescope. In addition, they are needed to characterize the performance of the telescope.
This section will describe and derive the formulas needed (see also Baars 1973, Kraus 1984, Downes 1989, Gordon et al. 1992).

3.1 The flux density of a calibration source

The **flux density** $S_{\nu,tot}$, the power radiated per unit area and per unit frequency, of a radio source at a given frequency is given by

$$S_{\nu,tot} = \int_{\Omega_S} B_\nu(T_B) d\Omega = \frac{2k}{\lambda^2} \int_{\Omega_S} J_\nu(T_B) d\Omega \tag{9}$$

where Ω_S is the source solid angle and T_B is the Planck brightness temperature of the source. $J_\nu(T_B)$ is the Rayleigh-Jeans brightness temperature at the frequency ν:
$J_\nu(T_B) \equiv T_{RJ} = \frac{h\nu}{k}(exp(\frac{h\nu}{kT_B}) - 1)^{-1}$, where λ is the wavelength of observation and k is the Boltzman constant.
The primary calibration sources are planets. For a source with uniform temperature and the shape of a disk of diameter θ_s the flux density equals

$$S_{\nu,tot} = \frac{2k}{\lambda^2} \frac{\pi}{4} \theta_s^2 J_\nu(T_B). \tag{10}$$

The telescope receives the flux through the signal and image sideband weighted by the sideband gain ratio. The flux of a planet thus is
$S_{tot} = [S_{tot}(\nu_{lsb}) + G_{\rm im} S_{tot}(\nu_{usb})]/(1 + G_{\rm im})$.
The difference between the lower sideband flux density $S_{tot}(\nu_{lsb})$ and the upper sideband flux density $S_{tot}(\nu_{usb})$ can be as large as $\sim 10\%$ due to the ν^2 dependence of S and given the IF frequencies at the 30m RT. The accuracy of the calculated fluxes (and aperture efficiencies, see below) thus depend on a good knowledge of the gain ratio.

3.2 The measured antenna temperature

The **antenna temperature**, only corrected for atmospheric losses (but not for rearward losses) is given by the convolution integral

$$T'_A(\theta,\phi) = \frac{1}{\Omega_A} \int_{source} P(\theta-\theta',\phi-\phi') J_\nu(T_B) \psi(\theta',\phi') d\Omega' \tag{11}$$

where $P(\theta,\phi)$ is the antenna diagram. The brightness distribution of the source is $J_\nu(T_B)\psi(\theta,\phi)$, with $\psi(0,0) = 1$, and the solid angle of the antenna pattern is
$\Omega_A = \int_{4\pi} P(\theta,\phi) d\Omega$.

Using the relation

$$\lambda^2 = A_{\rm eff} \Omega_A \tag{12}$$

(e.g. Kraus 1984), where $A_{\rm eff} = \eta_A A_{\rm geom} = \eta_A \pi (D/2)^2$ is the effective area of an antenna with diameter D and aperture efficiency η_A (see §3.3), and assuming a uniform disk temperature, leads to

$$\begin{aligned} T'_A(\theta,\phi) &= \frac{S_{\nu,tot} A_{\rm eff}}{2k} \frac{1}{\Omega_S} \int_{source} P(\theta-\theta',\phi-\phi') \psi(\theta',\phi') d\Omega' \\ &= \frac{S_{\nu,tot} A_{\rm eff}}{2k} \frac{\Omega_{\rm sum}}{\Omega_S} = \frac{S_{\nu,tot} A_{\rm eff}}{2k} K \end{aligned} \tag{13}$$

thereby defining the beam weighted source solid angle $\Omega_{\rm sum}$ and the correction factor K (Baars 1973).

For a **Gaussian beam** with HPBW θ_b

$$P(\theta) = \exp[-\ln 2 (2\theta/\theta_b)^2]$$

centered on a uniform source disk

$$\psi(\theta) = \begin{cases} 1 & \text{for } \theta \le \theta_s/2 \\ 0 & \text{else} \end{cases}$$

the integral eq. (11) can be rewritten:

$$T'_A(\theta=0) = \frac{1}{\Omega_A} 2\pi J_\nu(T_B) \int_0^{\theta_s/2} \exp\left[-\ln 2 (2\theta/\theta_b)^2\right] \theta d\theta$$

where θ_s is the diameter of the disc and θ_b is the half power beam width. (Here we used the approximation $sin\theta = \theta$.) The integration results in:

$$T'_A(\theta=0) = \frac{\Omega_{\rm mb}}{\Omega_A} J_\nu(T_B) \left[1 - \exp(-x^2)\right] \quad \text{with} \quad x = \sqrt{\ln 2}\ \ \theta_s/\theta_b \tag{14}$$

and with the beam solid angle $\Omega_{\rm mb}$. For a Gaussian beam we find:

$$\Omega_{\rm mb} = \int_{mb} P(\theta) \theta d\theta = \frac{1}{4 \ln 2} \pi \theta_b^2 \approx 1.133 \theta_b^2. \tag{15}$$

Eqs. (9, 12, 14) then lead to:

$$T'_A = \frac{S_{\nu,tot} A_{\rm eff}}{2k} K \quad \text{with} \quad K = \frac{1 - \exp(-x^2)}{x^2} \le 1.$$

valid for a Gaussian beam with HPBW θ_b and a disklike source of diameter θ_s.
The factor K corrects for the reduction in antenna temperature when observing a source which has a non-negligible diameter compared to the half power beam width. (For $\theta_s/\theta_b = 0.5$ the correction K is 9%.)

3.3 The aperture efficiency

The **aperture efficiency** η_A is defined as the ratio between the effective antenna area $A_{\rm eff}$ and geometrical area of the aperture $A_{\rm geom} = \pi(D/2)^2$ where D is the diameter of the telescope.
For the 30m radiotelescope ($2k/A_{\rm geom}$) is 3.906 Jansky per Kelvin. Per default the IRAM observing program outputs antenna temperatures T_A^* (also chosen with the `OBS` command `set scale antenna`) corrected for the atmosphere and rearward losses $F_{\rm eff}$: $T_A' = T_A^* F_{\rm eff}$. By defining the **flux density per beam** as $S_{\nu,b} \equiv K \times S_{\nu,tot}$ we get

$$\boxed{\eta_A = 3.906 \times \frac{T_A^*[\mathrm{K}]\ \mathrm{F_{eff}}}{S_{\nu,b}[\mathrm{Jy}]} \qquad \text{for the 30m telescope.}} \tag{16}$$

Note that, for pointlike sources with $\theta_s \ll \theta_b$, the aperture efficiency is independent of the beam width θ_b.
The flux per Kelvin on the T_A^* scale is

$$3.906 \times \frac{F_{\rm eff}}{\eta_A} \qquad \left[\frac{\mathrm{Jy}}{\mathrm{K}}\right] \tag{17}$$

3.4 The main beam efficiency

The **main beam efficiency** $B_{\rm eff}$ is defined as

$$B_{\rm eff} = \frac{\Omega_{\rm mb}}{\Omega_A} \qquad \text{with} \qquad \Omega_{\rm mb} = \int_{\rm mb} P(\theta,\phi)d\Omega$$

which is the percentage of all power received which enters the main beam.
Together with eq. (13) and for a disk shaped source which completely fills the main beam ($\Omega_{\rm sum} = \Omega_{\rm mb}$) we find, without assumptions about the beam shape: $T_A' = B_{\rm eff} J_\nu(T_B)$.

Using also eq. (14) and assuming a clean Gaussian beam we find:

$$T_A' = B_{\rm eff} T_{\rm mb} \qquad \text{with} \qquad T_{\rm mb} = J_\nu(T_B)\Big[1 - \exp\Big[-\ln 2\Big(\frac{\theta_s}{\theta_b}\Big)^2\Big]\Big].$$

The main beam efficiency can be estimated from the measured antenna temperature of a planet of known brightness temperature and diameter:

$$\boxed{B_{\rm eff} = \frac{T_A'}{T_{\rm mb}} = \frac{T_A^* F_{\rm eff}}{J_\nu(T_B)\big[1 - \exp(-x^2)\big]} \qquad \text{with} \qquad x = \sqrt{\ln 2}\ \ \theta_s/\theta_b.} \tag{18}$$

For pointlike sources ($\theta_s \ll \theta_b$), the main beam efficiency becomes very sensitive to small deviations from a Gaussian beam. The main beam efficiency is thus better derived from observations of a source which has a diameter comparable to that of the beam.
The -20 dB width of a Gaussian beam is just $\theta_{-20dB} = 2.58\ \theta_b$. Note that the factor $(1 - \exp(-(\sqrt{\ln 2}\ \theta_s/\theta_b)^2)^{-1}$ in eq. (18) is smaller than 1.01 for a source which is a factor of 2.58 larger than the HPBW.
For an extended source ($\theta_s \geq 2.6\theta_b$) and a clean Gaussian beam (that is a source completely filling the beam: $\Omega_{\rm sum} = \Omega_{\rm mb}$) we thus find to a good accuracy $T_{\rm mb} = J_\nu(T_B)$, and

$$B_{\rm eff} = \frac{T'_{\rm A}}{J_\nu(T_B)}. \tag{19}$$

The antenna diagram of a real telescope shows sidelobes and errorpatterns. Measuring sources which are larger than the beam size and using eq. (19) will thus lead to an effective beam efficiency $B'_{\rm eff}$ variing with the size of the source. See e.g. Gordon et al. (1992, p.340) for a discussion of the implications for the observer.

The **aperture - and the main beam efficiency** are related via the illumination (assuming a Gaussian beam):

$$\boxed{B_{\rm eff} = \eta_{\rm A}\frac{A_{\rm geom}\Omega_{\rm mb}}{\lambda^2} = 2.092\times10^{-5}\ \eta_{\rm A}\ \left[\theta_b\frac{D}{\lambda}\right]^2 \qquad \text{for the 30m telescope}} \tag{20}$$

with the aperture efficiency $\eta_{\rm A}$,
the half power beam width θ_b in [arcsec],
the diameter of the telescope D in [m],
and the wavelength of observation λ in [mm].

3.5 The forward efficiency

In a skydip, the total power on the sky is measured at equally spaced airmasses $A = 1/\sin(El)$. The skydip outputs several calibrated antenna temperatures on the sky $T^{\rm sky}_{\rm A,i}(A_{\rm i}) = F_{\rm eff}T_{\rm sky}(A_{\rm i}) + (1-F_{\rm eff})T_{\rm cab}$ (eq. 3). With eq. (4) we find

$$T_{\rm sky} = \frac{T^{\rm s}_{\rm ATM}(1-\exp(-\tau_{\rm s}(W)A)) + T^{\rm i}_{\rm ATM}(1-\exp(-\tau_{\rm i}(W)A))*G_{\rm im}}{1+G_{\rm im}}.$$

The rearward losses described by $F_{\rm eff}$ at different elevations are more or less constant. Thus the forward efficiency can be derived independently of the amount of precipitable water vapour W by a least squares fit to the model function. The atmospheric model ATM (Cernicharo 1988) is essentially used to derive values for the mean atmospheric brightness temperatures $T_{\rm ATM}$. See André & Cernicharo (1989) for a detailed description and error analysis of this procedure.

3.6 The half power beam width `HPBW`

Parameters like the flux per beam, the aperture- and the main beam efficiency depend on the knowledge of the half power beam width of the antenna pattern.

3.6.1 Small sources

The half power beam width θ_b at a given wavelength can be estimated from the FWHM measured on a source of known diameter θ_s. For disk shaped sources which are smaller than the half power beam width ($0 \le \theta_s/\theta_b \le 1$) the HPBW is simply given (Baars 1973) by:

$$\boxed{\theta_b = \sqrt{\theta^2_{\rm fwhm} - \frac{\ln 2}{2}\theta^2_s}} \tag{21}$$

Note: For a source which is as large as the HPBW, the FWHM derived with the above formula is 2.6% smaller than the exact FWHM derived with eq. 22.

3.6.2 Disklike sources of arbitrary size

For the general case, the two-dimensional convolution integral (eq. 11) of a Gaussian beam P and a disklike source v has to be solved. This is simplified by using the convolution theorem, which states that the fourier transform (FT) of the convolution is the product of the individual fourier transforms: $T^{FT}(u) = P^{FT}(u) \times v^{FT}(u)$. (Ref.: 'The Fourier Transform and its Applications' by R.N. Bracewell, McGraw-Hill, chapter 12). Another more direct approach is given by Harris (1988).
The FTs are:

$$P^{FT}(u) \propto \exp\left(-u^2 \frac{\theta_b^2}{16 \ln 2}\right) \quad \text{and} \quad v^{FT}(u) \propto \frac{J_1(\theta_s u/2)}{u}$$

Here J_1 and J_0 are the Bessel functions of first kind and of order 1 and 0. The backward transformation of the product of the FTs is simplified because both two-dimensional functions show circular symmetry. The convolution integral is:

$$T(\theta) = \int_0^\infty T^{FT}(u) J_0(\theta u) u du$$

where θ gives the distance between the center of the Gaussian beam and the disklike source. This integral can be rewritten (defining $R = \theta_s/\theta_b$):

$$T(\theta) \propto \int_0^\infty J_1\left(\frac{Ru}{2}\right) J_0\left(\frac{\theta u}{\theta_b}\right) \exp\left(\frac{-u^2}{16 \ln 2}\right) du \tag{22}$$

Note that the temperature in the center at $\theta = 0$ was already given by eq. (14). The FWHM of the convolved function $T(\theta)$ can be calculated numerically.

3.6.3 Extended sources

For extended disklike sources ($\theta_s \gg \theta_b$) the convolution problem is reduced to the convolution of a Gaussian beam with a straight edge. The convolution integral is

$$T(\theta) = \int_{\theta-\theta_s/2}^{+\infty} \int_{-\infty}^{+\infty} \exp\Big(-\frac{4 \ln 2}{\theta_b^2}(x^2+y^2)\Big) dy dx \qquad \Leftrightarrow$$

$$T(\theta) = \sqrt{\frac{4 \ln 2}{\pi \theta_b^2}} \int_{\theta-\theta_s/2}^{+\infty} \exp\Big[-\ln 2 (2x/\theta_b)^2\Big] dx = \Omega_{\rm mb}^{-0.5} \int_{\theta-\theta_s/2}^{\infty} P(x) dx$$

where θ is the displacement from the center of the beam to the center of the source. $P(x)$ again is the Gaussian beam function. For extended sources the derivation of the convolution integral directly yields the beam function.
Note: A source five times larger than the beam is well approximated by a straight edge. The difference between the exact FWHM of the convolved function (eq. 22) and the FWHM derived by assuming a staight edge is only 1.4% in this case.

4 Planets for the derivation of telescope parameters

Some of the planets are good calibrators because their temperatures and fluxes are well known. This section gives short remarks about the quality of the individual planets as calibrators and it presents a list of brightness temperatures. The main aim is to establish some agreement, especially within the IRAM 30m RT staff, on which planets, planetary temperatures, and procedures to use for calibration.

- **Mercury:**
  - Angular diameter varies between 3″ and 12″ approximately.
  - Large, fast phase effect. Therefore not used.
- **Venus:**
  - Angular diameter varies between 12″ and 65″ approx..
  - No phase effect seen at millimeter wavelengths (Greve priv. commun.).
- **Mars:**
  - One of the two most important primary calibrators, except when near opposition.
  - Diameter varies between 3″ and 25″(!) approx..
  - Measurements indicate that Mars is a near blackbody in the millimeter and submillimeter region because of its solid surface and tenuous atmosphere (Griffin et al. 1986).
  - It shows strong but narrow ^{12}CO and ^{13}CO absorption lines.
  - Duststorms on Mars might influence its brightness temperature.
  - Its temperature varies with heliocentric distance R [a.u.]. The distance dependence is given by $T_B = \langle T_B \rangle \sqrt{1.524/R}$ [K], where $\langle T_B \rangle$ is the brightness temperature at the mean distance to the sun of 1.524 a.u. (Ulich 1981).
- **Jupiter:**
  - Its angular diameter varies between 32″ and 42″ approx..
  - It has strong atmospheric absorption lines from NH_3, PH_3 (Griffin et al. 1986, Lellouch et al. 1984) which may especially influence observations with small bandwidth at or close to the line frequencies.
  - It is bright and its flux density does not vary with time.
  - Brightness temperatures are well known.
- **Saturn:**
  - The changing tilt angle of the rings as seen from the earth leads to a variation of its emission which may not be negligible.
  - Its ellipticity ϵ of 0.096 (Hildebrand et al. 1985) may not be negligible. ($\epsilon = (R_{\rm eq} - R_{\rm p})/R_{\rm eq}$, where $R_{\rm eq}$ and $R_{\rm p}$ are the equatorial and polar radii.)
  - Its angular diameter varies between 15″ and 20″ approx..
  - It is bright and its flux density does not vary with time.
  - It also has strong atmospheric absorption lines (see Jupiter).
- **Uranus:**
  - One of the two most important primary calibrators. It is weak, however.
  - Diameter is approx. 3″.
  - Brightness temperatures in the millimeter/submillimeter region are well known.
  - It may have atmospheric absorption lines of CH_4 (Orton et al. 1986). No CO or HCN has been detected so far (Marten et al. 1993).

- **Neptune:**
  - It is weaker than Uranus and it is found near Uranus on the sky for the next couple of years.
  - Diameter is approx. 3″.
  - It shows broad CO absorption- and HCN emission lines (Marten et al. 1993, Guilloteau et al. 1993b).
  - Note the discrepancy between the temperatures presented by Griffin & Orton (1993) and those found by Marten et al. (1993).

Table 1: Frequencies of some planetary atmospheric lines which should be avoided when using planets as calibrators

80-115 GHz (3mm Rec.)	120-170 GHz (2mm Rec.)	200-270 GHz (1.3mm Rec.)	300-370 GHz (0.8mm Rec.)
82.0 CH_4		220.4 ^{13}CO	330.6 ^{13}CO
82.9 CH_4		230.5 ^{12}CO	345.8 ^{12}CO
88.6 HCN		265.9 HCN	354.5 HCN
94.1 CH_4		~270 PH_3	
95.2 CH_4			
98.3 CH_4			
110.2 ^{13}CO			
115.3 ^{12}CO			

NH_3 does not have any lines in the frequency ranges of interest.

In order to derive telescope efficiencies and half power beam widths, the antenna temperature T_A^* and the FWHM $\theta_{\rm fwhm}$ are usually derived from a Gaussfit to a pointing continuum scan. The program `planflux.f` uses the source diameter θ_s for the date of observation, interpolates Rayleigh-Jeans brightness temperatures $J_\nu(T_B)$ from the table, and calculates the flux density per beam $S_{\nu,b}$. It may also calculate the half power beam width and efficiencies. The program takes into account the planets ellipticity, the variation of the Martian temperatures with heliocentric distance. It assumes planetary disks of uniform brightness. It does not take into account phase effects, polar inclination angles, or the effects of the Saturn rings. (The polar inclination angle is the angle between the planet pole and the line of sight. It might be important for planets with non-negligible ellipticity and non-negligible axis inclination, e.g. Saturn.)

The effective size of some planets is frequency dependent because of the planets atmospheric opacity. This small effect is also neglected by `planflux`. The program uses the angular planetary semi-diameters S.D. [″] at unit distance of one astronomical unit (Tab.3) given in the Astronomical Almanac (1987, E43).

Table 2: Planetary Brightness Temperatures T_B

Frequency	Wavelength	Mars	Jupiter	Saturn	Uranus[3]	Neptune[3]
[GHz]	[mm]	[K]	[K]	[K]	[K]	[K]
90	3.33	207[2]	179[1]	153[1]	134.7	129.8
150	2.00	210[4]	173[4]		111.8	107.1
227	1.32	213[4]	171[4]		97.7	93.0
310	0.97			135[5]	88.8	84.2
337	0.89	215[4]	174[4]		86.7	82.0

References: **(1)** 86.1 GHz values of Ulich et al. (1980), **(2)** Ulich (1981), **(3)** empirical fits given by Griffin & Orton (1993), see also Orton et al. (1986). Note that the Neptune temperatures differ from those found by Marten et al. (1993). **(4)** Griffin et al. (1986), **(5)** Hildebrand et al. (1985).
The above temperatures are derived from bolometric measurements with bandwidths of typically several 10 GHz! **Note that the Martian temperatures are brightness temperatures at the mean distance to the sun of 1.524 a.u.!** The Martian temperatures have an uncertainty of about 5% (Griffin & Orton 1993). The absolute calibration error of the observations which are based upon the Martian temperatures is estimated to be 10% (Griffin et al. 1986).

Table 3: Planetary Semi-Diameter

	Mercury	Venus	Mars	Jupiter	Saturn	Uranus	Neptune
S.D. [″]	3.36	8.34	4.68	95.25	78.28	35.02	33.50
R [km]	2437	6049	3394	69083	56775	25399	24297

5 Measured IRAM 30m telescope parameters

The following beam parameters were derived in 1994 by continuum cross scans on Mars and Uranus and by skydips using the IRAM heterodyne SIS receivers (Tab. 4, cf Kramer & Wild 1994). Subsequent measurements in 1995 and 1996 confirmed these data, within the observational accuracy.
The skydips were used to estimate forward efficiencies. From the planetary scans we derived half power beam widths, aperture, and main beam efficiencies, using formulas and planetary temperatures compiled above. The planets were nearly pointlike during the time of observations, diameters ranged between 3.5″ and 5.5″. For comparison we also derived moon efficiencies at full moon from lunar data (partly presented in Greve et al. 1997) using average brightness temperatures at the moon center from Linsky (1973) and formula from Mangum (1993). Note that moon efficiencies are equal to forward efficiencies. From the scatter of the day-to-day measurements we estimate errors of the efficiencies to be about ±10%. For a description and discussion of the errorbeam I refer to Greve et al. (1997) (cf. Garcia-Burillo et al. 1993).

ν_{dsb} [GHz]	HPBW [″]	η_A [%]	$B_{\rm eff}$ [%]	$M_{\rm eff}$ [%]	$F_{\rm eff}$ [%]	S_ν/T_A^* [Jy/K]
90	26.6	60	75	90	92	6.0
100	24.0	58	70	–	92	6.2
110	21.8	57	68	–	92	6.3
130	18.4	47	58	–	90	7.5
150	16.0	43	52	90	90	8.2
160	15.0	41	50	–	90	8.6
220	10.9	35	41	–	86	9.6
230	10.4	32	39	86	86	10.5
240	10.0	29	37	–	86	11.6

Table 4: IRAM 30m telescope efficiency data at the double sideband frequencies ν_{dsb}. The columns give the HPBW of the main beam and the following efficiencies : aperture, main beam, moon, and forward. The last column gives the flux density per antenna temperature ratio for a point source, which is $S_\nu/T_A^* = 3.906 \cdot F_{\rm eff}/\eta_A$ [Jy/K] for the 30m telescope.

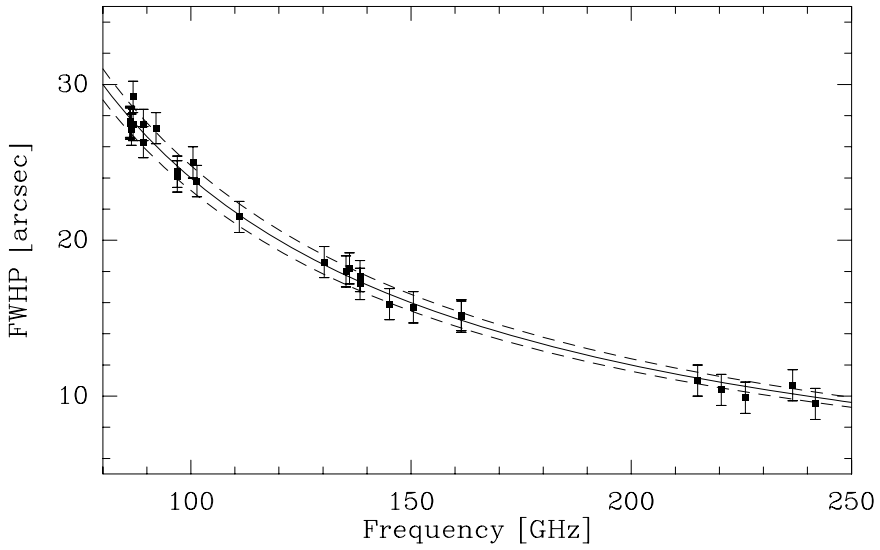

Figure 1: Half power beam widths (HPBW) as derived from planetary observations at the 30m telescope in the frequency range from 90 to 240 GHz. Observations were done during 1994 and presented in Kramer & Wild (1994). The accuracy of the observations is better than 1″ (dashed lines). The drawn curve corresponds to Eq. 23.

5.1 Half power beam widths

The product of measured beam width and frequency is nearly constant for frequencies up to 240 GHz (Fig. 1):

$$\mathrm{HPBW/[arcsec]} \cdot \nu/\mathrm{[GHz]} = (2400 \pm 80) \tag{23}$$

The error is the standard deviation of the product. The formula translates into HPBW= $(1.16 \pm 0.04) \cdot \lambda/D$ in radian with the diameter of the telescope D. A constant value indicates a constant illumination of the subreflector, i.e. a constant edge taper, independent of the receiver. The prefactor 1.16 is weakly dependent on the edge taper T_E (Goldsmith 1982):

$$\mathrm{HPBW} = 0.8\sqrt{T_E}\frac{1}{\pi}\alpha\left(T_E\right) \cdot \frac{\lambda}{D}. \tag{24}$$

The factor $\alpha(T_E)$ corrects for the influence of the subreflector. Goldsmith tabulates values between $T_E = 5$ and $T_E = 30$ dB. A prefactor of 1.16 ± 0.04 corresponds to an edge taper of $T_E = (11 \pm 3)$ dB. Note that the beam width is rather insensitive to the edge taper (Eq. 24). A higher value of the edge taper, i.e. a stronger gradiation, would lead to a lower sidelobe level and a higher beam efficiency. On the other hand, it would also lead to a lower aperture efficiency (e.g. Rohlfs & Wilson 1996, p.140). An edge taper of 11 dB thus is a compromise between these two aims.

5.2 Aperture efficiencies

From the aperture efficiencies we can estimate the tapered surface rms-value σ_s via the Ruze formula,

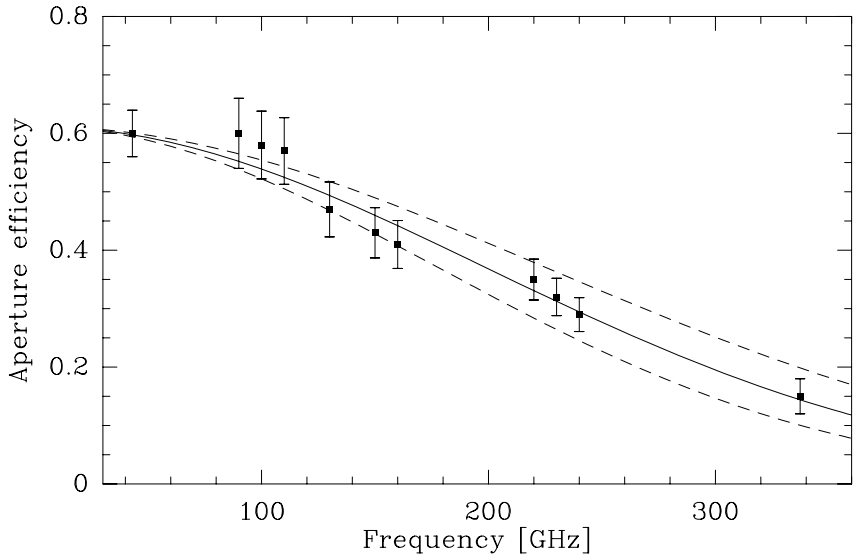

Figure 2: Aperture efficiencies η_A as derived from observations of small planets at the 30m telescope in the frequency range 43 to 337 GHz. Greve et al. (1994) found $\eta_A = 60 \pm 7\%$ at 43 GHz. Kramer & Wild (1994) presented efficiencies in the range 90–240 GHz with an accuracy of $\sim 10\%$. In January 1995 we measured the efficiencies at 337 GHz finding $\eta_A = 0.15 \pm 20\%$. The inner curve corresponds to the fitted rms value of 85 μm. The outer, dashed curves correspond to rms values of 75 and 95 μm.

$$\eta_A = \eta_{A0} \cdot \exp\left(\frac{-16\pi^2\sigma_s^2}{\lambda^2}\right) \tag{25}$$

assuming that η_{A0} is independent of the wavelength λ, i.e. the illumination of the subreflector is constant (Eq. 23). Fig. 2 shows aperture efficiencies in the range 43 to 337 GHz. A linear least-squares fit to the linearized Eq. 25 results in $\eta_{A0} = 0.62$ and $\sigma_s = 85\mu$m. This agrees with phase-coherent holographic measurements of the surface which indicate $\sigma_s = 80 \pm 20\mu$m (Morris et al. 1996). It also agrees with values derived from drift scans across the moon edge (Greve, Kramer, Wild 1997).

From Eq. 25 alone, we see that the aperture efficiency at 230 GHz would improve significantly by 32 %, from 0.32 to 0.42, when the surface accuracy σ_s is improved by 20 μm from 85μm to 65μm.

Acknowledgements

I am grateful to Dennis Downes, Albert Greve, Dave Morris, Andreas Schulz, and Wolfgang Wild for comments and discussions. André Marten and Stephane Guilloteau contributed useful comments on planets and their temperatures.

References

[1] André, Ph., Cernicharo, J. 1989, 'Report on Skydips made during Test Week 23', IRAM Internal Report

[2] Baars, J.W.M. 1973, IEEE Transactions on Antennas and Propagation, Vol. Ap-21, No. 4, 'The Measurement of Large Antennas with Cosmic Radio Sources'

[3] Cernicharo, J. 1988, Docteur d'Etat es Sciences, Université de Paris VII

[4] Downes, D. 1989, 'Radio Astronomy Techniques' in "Evolution of Galaxies, Astronomical Observations", eds. I. Appenzeller, H.J. Habing, P. Léna, Springer Verlag, Heidelberg

[5] Garcia-Burillo, S., Guélin, M., Cernicharo, J. 1993, A&A, 274, 144

[6] Goldsmith, P.F. 1982, Quasi-Optical Techniques at Millimeter and Submillimeter Wavelengths, in: Button, K.J. (ed.), Infrared and Millimeter Waves, Vol. 6: Systems and Components, Academic Press, New York, pp. 277-343

[7] Gordon, M.A., Baars, J.W.M., Cocke, W.J. 1992, A&A, 264, 337, 'Observations of radio lines from unresolved sources: telescope coupling, Doppler effects, and cosmological corrections'

[8] Greve, A., Steppe, H., Graham, D., Schalinsky, C.J. 1994, A&A, 286, 654

[9] Greve, A., Kramer, C., Wild, W. 1997, A&AS, in preparation

[10] Griffin, M.J., Ade, P.A.R., Orton, G.S., Robson, E.I., Gear, W.K., Nolt, G., Radostitz, J.V. 1986, Icarus, 65, 244, 'Submillimeter and millimeter observations of Jupiter'

[11] Griffin, M.J., Orton, G.S. 1993, Icarus, 105, 537, 'The Near-Millimeter Brightness Temperature Spectra of Uranus and Neptune'

[12] Guilloteau, S. 1987, 'Spectral Line Calibration on the 30m and 15m Antennas'

[13] Guilloteau, S. 1993, 'IRAM Plateau de Bure Interferometer - Amplitude Calibration'

[14] Guilloteau, S., Dutrey, A., Marten, A., Gautier, D. 1993, A&A , 279, 661, 'CO in the Troposphere of Neptune - Detection of the J=1-0 line in absorption'

[15] Harris, A.I. 1988, International Journal of IR and mm Waves, V.9

[16] Hildebrand, R.H., Loewenstein, R.F., Harper, D.A., Orton, G.S., Keene, J. 1985, Icarus, 64, 64, 'Far infrared and submillimeter brightness temperatures of the giant planets'

[17] Klein, M.J., Janssen, M.A., Gulkis, S., Olsen, E.T. 1978, in 'The Saturn System', D.M. Hunten and D. Morrison, Eds., Springfield, VA: Nat. Tech. Inform. Ser., pp. 195-216, 'Saturn's microwave spectrum: Implications for the atmosphere and the rings'

[18] Kramer, C., Wild, W. 1994, 'Efficiencies at the 30m telescope', IRAM Newsletter No. 18

[19] Kraus, J.D. 1984, Cygnus-Quasar Books, 'Radio Astronomy'

[20] (K&U) Kutner, M.L., Ulich, B.L. 1981, ApJ, 250, 341, 'Recommendations for Calibration of Millimeter-Wavelength Spectral Line Data'

[21] Lellouch, E., Encrenaz, T., Combes, M. 1984, A&A, 140, 405

[22] Linsky, J.L. 1973, ApJS, 216, 25, 163

[23] Mangum, J.G. 1993, PASP, 105, 117

[24] Marten, A., Gautier, D., Owen, T., Sanders, D.B., Matthews, H.E., Atreya, S.K., Tilanus, R.P.J., Deane, J.R. 1993, ApJ, 406, 285, 'First observations of CO and HCN on Neptune and Uranus at Millimeter Wavelengths and their Implications for Atmospheric Chemistry'

[25] Morris, D., Lazareff, B., Lamb, J., Zweigle, J., Mattiocco, F., Penalver, J., Navarro, S., Carter, M. 1996, 'Phase-coherent holography of the 30m telescope in September 1996', IRAM report

[26] Orton, G.S., Griffin, M.J., Ade, P.A.R., Nolt, I.G., Radostitz, J.V., Robson, E.I., Gear, W.K. 1986, Icarus, 67, 289, 'Submillimeter and millimeter observations of Uranus and Neptune'

[27] Rohlfs, K., Wilson, T.L. 1996, 'Tools of Radio Astronomy', Springer-Verlag, Berlin

[28] Stutzman, W.L., Ko, H.C. 1974, IEEE Transactions on Antennas and Propagation, 403, 'On the measurement of antenna beamwidth using extraterrestrial radio sources'

[29] Ulich, B.L., Haas, R.W. 1976, ApJS, 30, 247 'Absolute calibration of milimeter-wavelength spectral lines'

[30] Ulich, B.L., Davis, J.H., Rhodes, P.J., Hollis, J.M. 1980, IEEE Transactions on antennas and propagation, Vol. AP-28, No. 3, 'Absolute Brightness Temperature Measurement at 3.5-mm Wavelength'

[31] Ulich, B.L. 1981, A.J., 86, 1619, 'Millimeter wavelength continuum calibration sources'

[32] Wright, E.L. 1976, ApJ, 210, 250, 'Recalibration of the far-infrared brightness temperatures of the planets'

[33] Wright, E.L., Odenwald, S. 1980, Bull. Am. Astron. Soc., 12, 456, 'Brightness temperatures of Mars 1979-1983'